Chapter 12

MODELING MERISTIC CHARACTERS OF ASTERACEAN FLOWERHEADS

JOHANNES BATTJES
van Tuyll van
Serooskerkenplein 432
1076 LZ Amsterdam
The Netherlands

and

PRZEMYSLAW PRUSINKIEWICZ
Dept. of Computer Science
University of Calgary
2500 University Drive NW
Calgary, Alberta
Canada T2N 1N4

1. Introduction

1.1. *Symmetry and Organ Numbers in Plants*

According to Weyl (1952), the word *symmetry* commonly has two different meanings. In one sense, symmetry is defined as a group of transformations that map an object into itself. This usage is reflected in expressions such as bilateral or rotational symmetry. In a broader sense, "symmetric means something like well-proportioned, well-balanced, and symmetry denotes that sort of concordance of several parts by which they integrate into a whole. Beauty is bound with symmetry" (Weyl, 1952). We will use the word symmetry in this broader sense.

A conspicuous aspect of symmetry in plants is the *number of organs* of a particular type (meristic character) in flowerheads and flowers. The preference for a certain number is called *numerical canalization* (Huether, 1968; Bachmann, 1983; Vlot *et al.*, 1992) and is often closely related to the phyllotaxis of flowers and flowerheads. For example, flowers of the Brassicaceae have whorls of two or four organs, and the numbers of organs of different types are usually multiples of two (Endress, 1992). Similarly, flowerheads from the Asteracean genus *Mikania* have four florets per flowerhead inserted in two decussate pairs (King and Robinson, 1987). In contrast, the numbers of different floral organs in flowers of the

Ranunculaceae frequently vary among Fibonacci numbers (Endress, 1987). This preference for Fibonacci numbers occurs together with a Fibonacci-type spiral phyllotaxis of the flower (Meicenheimer, 1979). An equally tight relationship between spiral phyllotaxis and organ numbers exists in flowerheads of the Asteraceae (Weisse, 1897; Church, 1902; Hirmer, 1931; Battjes *et al.*, 1993). A distribution curve of the number of ray florets or phyllaries (involucral bracts) in a sample of heads from the same Asteracean species often has one or more peaks at Fibonacci numbers, and lower frequencies between these peaks (Ludwig 1887; later literature summarized in Battjes and Bachmann, in press). Only organs that are inserted in a single row at the rim of flowerheads show these remarkable non-random distributions (Battjes and Bachmann, in press). The preferred numbers of organs in predictable positions are thought to give Asteracean flowerheads their symmetric appearance (Hirmer, 1931; Dormer, 1972; Leppik, 1977).

A developmental explanation for numerical canalization is that the mechanism responsible for the formation of phyllotactic patterns in flowers or flowerheads is capable of dampening the effect of genetic and environmental variation on organ numbers. An indication of the validity of this hypothesis is the fact that whorled flowers exhibit less variation in numbers among and within species than flowers with spiral phyllotaxis (Endress, 1990). This suggests that different phyllotactic patterns may have different capacities for keeping organ numbers constant. The aim of this chapter is to clarify the relationships between the phyllotaxis of flowers and flowerheads, the preferred number of organs, and the degree of meristic variation. We focus on flowerheads of the Asteracean genus *Microseris* because their phyllotactic patterns are relatively easy to analyze, and their meristic variation has been extensively documented.

1.2. *Previous Work on the Relationship between Spiral Phyllotaxis and Numerical Canalization*

1.2.1. *Hirmer's Work and the Collision Model*

In many whorled flowers and in decussate flowerheads there is an obvious relationship between patterns of organ insertion and organ numbers, since each organ has a clearly defined position and associated identity. On the other hand, in flowerheads with spiral phyllotaxis it is more difficult to see why the numbers of organs at the periphery are canalized towards Fibonacci numbers, and when deviations from these numbers occur. Although several authors discussed the relationship between Fibonacci numbers of organs and spiral phyllotaxis in flowerheads (reviewed in Battjes and Bachmann, in press), Hirmer (1931) was the first to propose a convincing explanation. Selected ideas of Hirmer were captured and formalized in the *collision model* of phyllotaxis (Fowler *et al.*, 1992; Battjes, 1994), which is summarized below:

- Consecutive primordia are placed on the receptacle with a constant divergence angle of 137.5° with respect to each other, as seen from the receptacle's center. This value is assumed *a priori* in the model.

- Initially, primordia are placed on the circular rim at the circumference of the receptacle. This process takes place as long as there is enough space, that is, the distance between a new primordium and its closest previously placed neighbor exceeds a predefined threshold.
- A primordium that does not fit on the rim is translated radially towards the center or the apex of the receptacle, so that the distance between the new primordium and its closest neighbor is equal to the threshold value. This process continues until there is no space available on the receptacle.
- The developmental fate of primordia is determined by their position on the receptacle. Ray florets or inner phyllaries develop from primordia positioned on the rim of the receptacle.

Hirmer (also see Dormer, 1972) observed that the distance between neighboring primordia can become smaller than a critical threshold only after a Fibonacci number of primordia have been placed on the rim. This observation holds for any values of rim radius and threshold distance (see Appendix A for an elementary proof). Consequently, the collision model implies that the number of organs resulting from primordia placed on the rim will always be a Fibonacci number.

1.2.2. *Confirmation of the Collision Model*

It is not immediately obvious that the collision model is sufficient to explain the arrangement of primordia into smooth opposite parastichies. Nevertheless, computer simulations demonstrate the emergence of spiral patterns on receptacles of various shapes for a wide range of primordia sizes (Fowler *et al.*, 1992).

One implication of the collision model is that primordia are placed in circular rings, starting at the rim of the receptacle. In contrast, most other models of spiral phyllotaxis assume a continuously decreasing distance between consecutive primordia and the midpoint of the receptacle (e.g. Vogel, 1979; Erickson 1983; Jean, 1994). Observations confirm that Asteracean flowerheads exhibit some of the ring-like properties postulated by the collision model. Three-dimensional measurements of organ positions in *Micro seris pygmaea* have shown that there are sudden decreases in distance to the midpoint between primordia 13 and 14 and between primordia 26 and 27, numbered from the rim inwards. These decreases are significantly larger than the decrease between subsequent primordia within the outermost rings of 13 (Battjes *et al.*, 1993).

The collision model also postulates that the position of primordia with respect to the rim of the receptacle, rather than the ontogenetic order of initiation, determines the developmental fate during their differentiation. Again there are indications that this assumption is realistic. For flowers it is known that genes determining the de-velopmental fate of floral organs (sepals, petals, stamens, carpels) are expressed in rings. These expression patterns are thought to be independent of floral phyllotaxis, and thus of the ontogenetic order of primordia, because the identity of the organs

may change as a consequence of mutations, while the arrangement and number of organs remains constant (Coen and Carpenter, 1993). For flowerheads, Hirmer (1931) and Bachmann and Chambers (1990) postulated that the differential development of peripheral versus central primordia is determined by a concentration gradient that indicates the distance of a primordium from the rim. No gene expression patterns confirming this hypothesis have yet been found, but the existence of a gradient that provides positional information is likely. For example, during the early development of *M. pygmaea* flowerheads, primordia on the rim subdivide into an inner phyllary and a floret. This subdivision appears to be controlled by the distance from the rim rather than the strict ontogenetic order of the primordia (Battjes *et al.*, 1992).

1.2.3. *Discrepancies between Flowerhead Development and the Model*

Although the assumptions of the collision model discussed above are realistic, the model does not accurately capture several aspects of flowerhead phyllotaxis and meristic variation.

The divergence angle in the model is assumed to be constant, but observed angles vary considerably. For instance, *Microseris* exhibits divergence angles much lower than 137.5° at transitions between rings of 13 primordia. This phenomenon can be explained by assuming that a new primordium attempts to minimize the distance to both of its closest neighbors (Battjes *et al.*, 1993), rather than simply preserving a threshold distance to its nearest neighbor. Similar deviations from the average divergence angle after Fibonacci or Lucas numbers of florets were observed in *Helianthus* heads (Ryan *et al.*, 1991), although in that study numerical canalization was not considered. In vegetative shoots, regular deviations from the average divergence angle have been found as well, for example in subdecussate shoots (Dormer, 1972).

Another unrealistic assumption of the collision model is the absence of growth of the surface on which the phyllotactic pattern is generated. Flowerheads usually grow considerably in size during the initiation of involucral bracts and florets (Popham and Chan, 1952; Rauh and Reznik, 1953; Horridge and Cockshull, 1979; Palmer and Steer 1985; Sharman and Sedgley, 1988; Brown and Menary, 1994). For example, in a variety of sunflower the capitulum radius increased fivefold during the initiation of about 1500 bracts and florets (Palmer and Steer, 1985). In the much smaller flowerheads of *Microseris douglasii* with only 80 florets, the increase in circumference during floret initiation alone is almost twofold (Battjes and Bachmann, 1994). The diameter of the individual primordia also increases over time, although the measured growth rates are lower than those of the receptacle (Battjes *et al.*, 1994).

Finally, the collision model yields a strict preference for Fibonacci numbers of inner phyllaries, whereas observed numbers are canalized less rigidly. Organ numbers are more variable than numbers of parastichies (Battjes and Bachmann, in press), which in Asteracean flowerheads are almost always Fibonacci numbers

(Ryan *et al.*, 1991; Battjes *et al.*, 1993; Szymanowska-Pulka, 1994). Consequently, non-Fibonacci numbers of ray florets or inner phyllaries may occur in flowerheads with Fibonacci numbers of parastichies (Weisse, 1897). This aspect of flowerhead phyllotaxis is not captured by the collision model, although it is essential for an understanding of meristic variation in flowerheads.

1.3. *Objectives of the Current Work*

In the present paper we analyze in detail the relationship between spiral phyllotaxis and the number of organs in flowerheads. The central questions are:

- how can a non-Fibonacci number of inner phyllaries arise in a *Microseris* flowerhead with a Fibonacci number of parastichies, and
- what is the relationship between the ontogenetic order of primordia and their chance of developing into inner phyllaries.

We hypothesize that the answers to these questions can be found by introducing two modifications into the collision model, inspired by observations listed in Sec. 1.2.3. The first modification is the incorporation of receptacle growth during floret initiation. The second is the adjustment of divergence angles that maximizes local density of primordia packing on the suface of the receptacle. The model predicts that:

- receptacles with higher growth rates have more variable numbers of organs, and
- when the number of inner phyllaries is not a Fibonacci number, some primordia are likely to develop into inner phyllaries out of the ontogenetic order.

Two modes of receptacle growth were simulated and analyzed: uniform and non-uniform; the latter is characterized by a slower growth rate at the periphery of the head. To test the validity of the model, we compared floret and inner phyllary positions measured in *M. pygmaea* with the results of simulations. In both cases, the model is in agreement with observations of the positions of inner phyllaries in the flowerheads of *M. pygmaea*. The non-uniform growth model leads, however, to a more realistic distribution of organs on the receptacle.

2.The Modified Collision Model

2.1. *Placement of Primordia with Adjustments in the Divergence Angle*

In this paper, we consider two-dimensional, circular receptacles. We also conceptualize primordia as being circular, with a constant radius r. The position of primordium i at time t is specified by the *radius* $\rho_{i,t}$ (distance between the center of the primordium and the center of the receptacle) and *azimuth* $\psi_{i,t}$ (angle between

the position vector and a predefined direction). Time is measured in plastochrons, defined as intervals between the addition of consecutive primordia.

The placement algorithm attempts to maximize the local density of primordia on the receptacle while approximately preserving the divergence angle of 137.5° between subsequent primordia. The algorithm can be described most easily in terms of an *outward* motion of primordia seeking a stable position as far as possible from the receptacle's center. The azimuth of a new primordium $i \geq 1$ is initially set to $\psi_{i,t} = (i-1)137.51°$, and the distance $\rho_{i,t}$ is set to 0. The primordium is (conceptually) moved outward ($\rho_{i,t}$ gradually increases), until it reaches the rim or collides with a previously placed primordium (the distance between the centers of the new and the old primordium is equal to $2r$). In the first case the placement of primordium i is completed. In the second case the radius $\rho_{i,t}$ is further increased while the azimuth $\psi_{i,t}$ is adjusted to keep the distance between primordium i and the old primordium equal to $2r$. Intuitively, primordium i can be viewed as rolling along the edge of the colliding primordium. This process may be repeated for the subsequent colliding primordia encountered by primordium i during its motion, and continues until primordium i reaches the rim or assumes a stable resting position on two older primordia. By definition, a stable position is characterized by two conditions:

- primordium i is tangent to two older primordia, and
- the position vector of primordium i lies inside the wedge formed by the position vectors of these two older primordia.

The example shown in Fig. 1 clarifies the placement process. In its initial outward motion, primordium i first collides with primordium a (position 1), then rolls on a until a collision with primordium b occurs. The resulting position 2 is unstable,

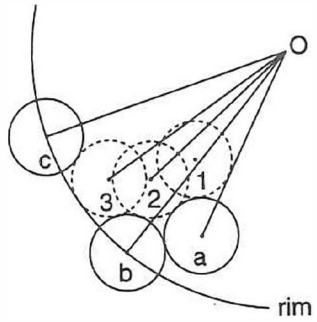

Fig. 1. Explanation of the algorithm for the positioning of primordia. A new primordium moves away from the center of the receptacle O towards the rim. After a collision with primordium a (position 1), the new primordium rolls over a until it collides with primordium b, then rolls on b until it collides with c. The resulting position 3 is stable and terminates the placement.

because the position vector of primordium 2 lies outside the wedge formed by the position vectors of primordia a and b. Consequently, primordium i rolls further on primordium b, until a collision with primordium c occurs. Position 3 achieved at this point is stable, because the position vector of primordium 3 lies inside the wedge formed by position vectors of primordia b and c. Notice that position 3 can be interpreted as the result of displacing primordium i *inward* with respect to its neighbors b and c, due to the lack of sufficient space between b and c on the rim. Thus, if we abstract from the details of the placement algorithm, the filling of the receptacle begins at the rim and proceeds in the general direction of the center of the receptacle, as observed in nature.

Figures 2–7 further illustrate the placement of primordia in the case of a non-growing receptacle. Filling the receptacle starts at the rim (Fig. 2). Primordia on the rim are subdivided into a floret and an inner phyllary. Initially, the divergence angle between consecutive primordia is equal to 137.5° (Fig. 3). Primordia are added to the rim until a collision between a new and existing primordium occurs (Fig. 4). The new primordium is then placed in a more inward position (Fig. 5), and the divergence angle is adjusted so that the new primordium rests stably on two older primordia (Fig. 6). The simulation stops when the receptacle is full (Fig. 7).

2.2. *Growth of the Receptacle*

The modified collision model makes it possible to incorporate expansion of the receptacle into the simulations (Figs. 8–11). We assume that the receptacle has a radius of R_1 at the beginning of primordia placement, and that the radius increases by a constant value c during each plastochron:

$$R_{n+1} = R_n + c \quad \text{for} \quad n \geq 1 . \tag{1}$$

Linear growth of the receptacle with the plastochron number has been assumed without a solid observational basis. Simulations indicated, however, that alternative formulas (for example, postulating multiplication of the radius by a constant factor rather than addition of a constant increment) lead to qualitatively similar results. Furthermore, note that the radius of the receptacle expressed by Eq. 1 may be a non-linear function of real time, if the duration of the plastochron changes.

Due to the rotational symmetry of a disk, the relative increase in circumference at a certain distance from a disk's center is equal to the relative increase in the radius at that distance. Consequently, specification of the radial growth is sufficient to characterize the expansion of the entire disk. The radial velocity $d\rho/dt$ of a point P on a growing disk is equal to the integral of the relative elementary rate of radius expansion $d(d\rho/dt)/d\rho$, taken between the center of the disk and the point under consideration (Erickson and Sax, 1956; Green and King, 1966). In the simplest case of *uniform growth*, the relative elementary rate of radius expansion is assumed to be constant all over the disk. Consequently, the distance $\rho_{P,t}$ between point P and the disk center remains in constant proportion to the disk radius R_t as the disk grows:

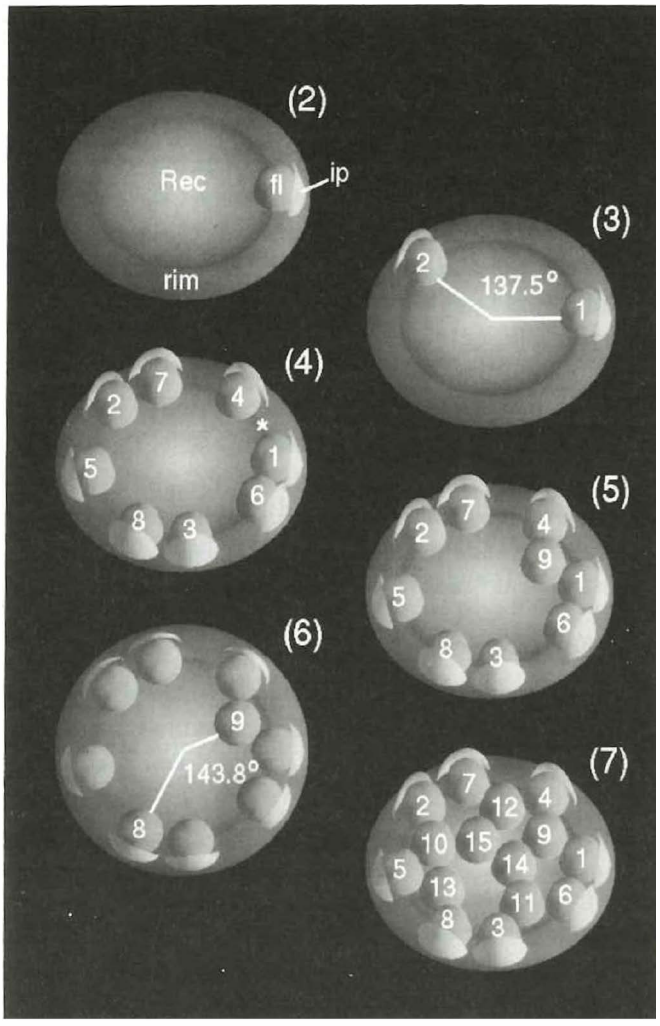

Figs. 2–7. Pattern formation on a static (non-growing) receptacle according to the modified collision model. (2) Like all primordia on the rim of the receptacle, the first primordium is divided into an inner phyllary (ip) and a floret (fl). (3) Initially, the divergence angle between subsequent primordia is equal to 137.5°. (4) After eight primordia have been placed on the rim, there is no space for the next primordium (*). (5) Primordium 9 is placed in a more inward position. (6) The position of primordium 9 is adjusted so that it rests on its two closest neighbors. As a result, the divergence angle deviates from 137.5°. (7) Receptacle filled with primordia.

$$\frac{\rho_{P,t+1}}{R_{t+1}} = \frac{\rho_{P,t}}{R_t}. \tag{2}$$

We also consider *non-uniform growth*, assuming that the relative elementary growth is slower in the outer zone of the receptacle, where primordia have already

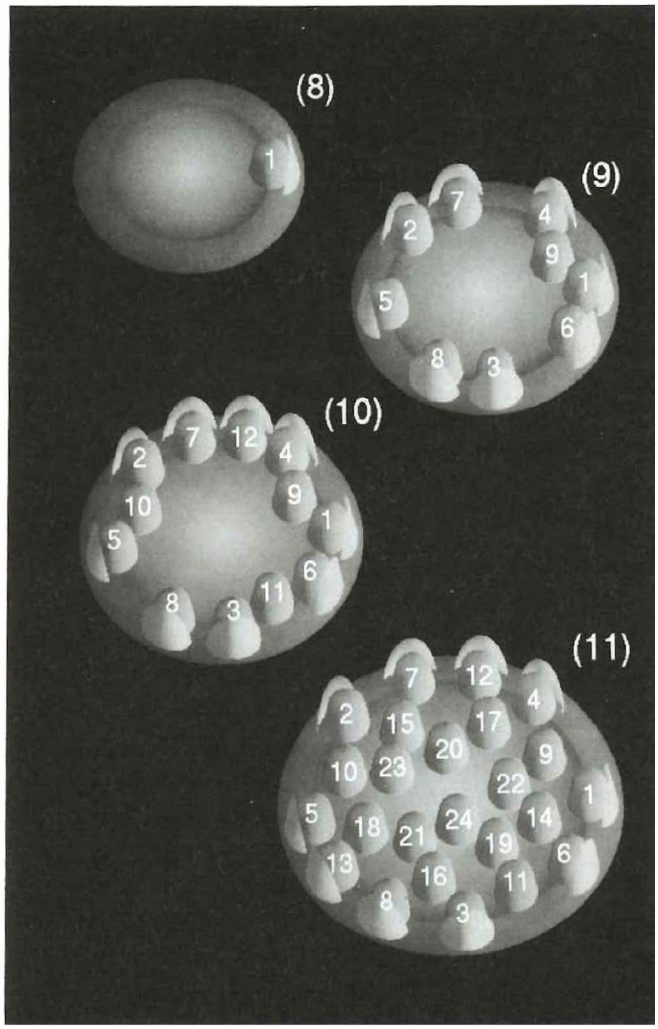

Figs. 8–11. Pattern formation on a growing receptacle. (8) The first primordium. (9) Primordium 9 is placed in a more inward position as in Fig. 6. (10) Due to the growth of the receptacle, primordia 12 and 13 fit again on the rim. (11) Receptacle filled with primordia.

been formed, than in the remaining inner part. In the extreme case of no growth in the zone with primordia, the distance between any point in this zone and the disk border is constant in absolute terms:

$$R_{t+1} - \rho_{P,t+1} = R_t - \rho_{P,t} \,. \tag{3}$$

The growth of the inner part of the receptacle is described as in the uniform case (Eq. 2). The above equations describe the growth of any point on the receptacle

and thus apply, in particular, to the points that represent the centers of primordia which are of focal interest in this paper.

3. Evaluation of the Modified Collision Model

In order to evaluate the modified collision model, we compared the results of simulations with the observations of *Microseris pygmaea* heads using three criteria:

- spatial arrangement of florets on the receptacle,
- numbers of inner phyllaries and their canalization, and
- ontogenetic order of inner phyllary positions.

The methods used for comparisons and the results are presented below.

3.1. *Spatial Arrangement of Florets on the Receptacle*

3.1.1. *Methods for Flowerhead Observations*

Immature flowerheads of *M. pygmaea* strain C96b ranging from 1.5 mm to 4 mm in diameter were collected in the greenhouse of the University of Amsterdam in 1991 and fixed in alcohol (Battjes *et al.*, 1992). The number of inner phyllaries per flowerhead ranged from 7 to 16, with the Fibonacci numbers 8 and 13 represented most frequently. A non-random sample of 47 heads with the numbers of inner phyllaries distributed as evenly as possible between 8 and 13 were embedded in glycol methacrylate, sectioned and stained using the PAS reaction, according to standard anatomical techniques (Fig. 12). The heads were then projected on graph paper using a *camera lucida* and drawn by hand. The floret and inner phyllary primordia were numbered in the ontogenetic order, determined by drawing opposite parastichies over primordia positions and counting the numbers of parastichies in each direction. In all heads, except one that was excluded from further analysis, these numbers were consecutive Fibonacci numbers. The ordering numbers were then assigned to primordia using the Bravais-Bravais theorem (Jean, 1994), which states that the ordering numbers of adjacent primordia on an n-parastichy differ by n. Since the Bravais-Bravais theorem characterizes differences between primordia numbers rather then their absolute values, an additional assumption was made that number 1 would denote the first floret with associated inner phyllary (Fig. 13).

The estimated positions of the centers of all primordia were recorded in Cartesian coordinates. Each inner phyllary was assumed to have the same number in the ontogentic order as the floret in its axil (Battjes *et al.*, 1992; also see Fig. 13). Positions of outer phyllaries were measured separately, since they do not have florets in their axils. These positions were not included in the further analysis of the spatial arrangement of florets on the receptacle, because the outer phyllaries are inserted below the rim of the receptacle, whereas our model is limited to the layout of primordia on a planar receptacle.

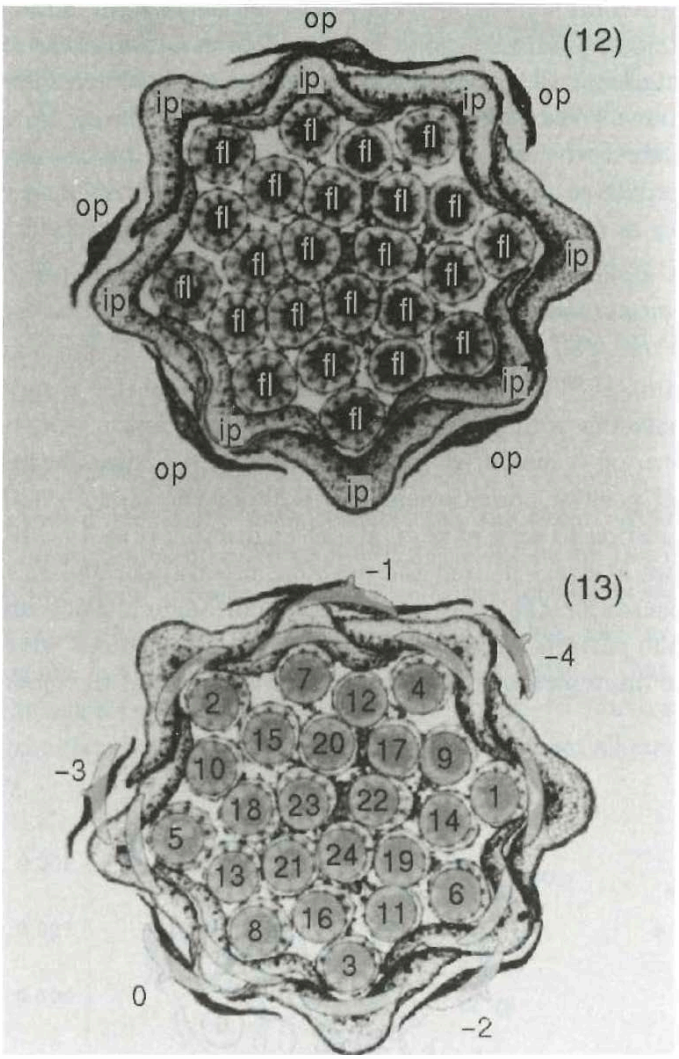

Figs. 12–13. Section through a flowerhead of *Microseris pygmaea*. (12) Identification of the organs: outer phyllaries (op), inner phyllaries (ip) and florets (fl). The inner phyllaries have florets in their axils, the outer phyllaries are not associated with florets. (13) The same head with superimposed symbols indicating measured organ positions. Florets are numbered in the ontogenetic order, starting at 1. The first eight florets are associated with the inner phyllaries. The outer phyllaries have been assigned numbers 0 to −4 by extending the ontogenetic order beyond the florets.

3.1.2. *Methods for Simulations*

Simulations were performed on a Silicon Graphics workstation using an in-house software implementation of the modified collision model. Different phyllotactic patterns were created by systematically varying three parameters described in Sec. 2.2: the initial radius of the receptacle R_1, the growth constant c, and the mode of receptacle growth (uniform or non-uniform). The ranges of the initial radius

(0.4 to 2.1 length units) and growth constant (0 to 0.06 length units) were chosen to yield floret numbers that correspond to those observed in *Microseris*. In one series of 20,000 simulations, each interval was represented by 100 evenly spaced samples, yielding simulated flowerheads with all the numbers of florets from 18 to 60. In another experiment, the results of 5000 simulations were used to visually represent the quality of pattern approximation, the number of florets, and the number of inner phyllaries as functions of growth parameters. In all simulations presented in this paper, r (the primordium radius) was set at 0.25 length units.

3.1.3. *Methods for Comparing Observed and Modeled Flowerheads*

Visual inspection is the most straightforward technique for comparing observed phyllotactic patterns with their models. To make it easier, we superimposed a modeled pattern on a measured pattern of primordium distribution, and interactively adjusted position, orientation, and scale of the model on the screen of a graphics workstation to achieve as good a fit as possible (Fig. 14). By making these adjustments, we abstracted from the position, orientation, and size of the flowerheads, and focused on the relative distances and angles, which are the essential attributes of the patterns. Differences in primordium positions which remain after fitting indicate discrepancies between the observations and the model.

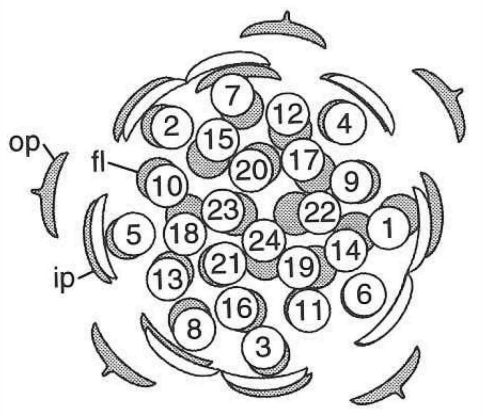

Fig. 14. A simulated head (light) superimposed on a measured head (dark) after the position, orientation, and scale of the model have been adjusted to achieve as good a fit as possible. Organ symbols are as in Fig. 12.

In order to speed up the process of fitting and to evaluate the results of the comparisons more objectively, we introduced the sum of squared distances (SSD) between corresponding primordium positions as a measure of discrepancy. We also developed an algorithm that minimizes the SSD automatically, by applying optimum transformations without human intervention (Appendix B). This algorithm was used to systematically compare families of simulated patterns with the observed flowerheads. The numbers of florets in the observed flowerheads ranged from 19

to 58, (Sec. 3.1.1) but not all intermediate numbers were present. Consequently, we subdivided the range of 18 to 60 florets into 14 equal intervals, and selected one flowerhead as the representative for each interval. Thus, the simulated patterns in the 18–60 floret range were compared to heads that had at most two florets more or less than the simulated pattern. The representative heads were characterized by small values of the SSD with respect to most other heads of a similar size, and in this sense they could be considered typical.

Different numbers of florets can be incorporated in the calculation of the SSD. We experimented with numbers ranging from 13 to the maximum number not exceeding the number of florets in the simulated or observed pattern (see Appendix B).

3.1.4. *Comparison Results*

To evaluate the overall similarity between simulated and observed patterns we incorporated the maximum number of primordium positions in the calculation of the SSD. Small deviations between simulated and observed heads were frequently found when the growth constant was larger than zero. Thus, the incorporation of receptacle expansion in the model leads to a simulated pattern that more closely approximates the observed phyllotactic pattern. Figure 15 illustrates this phe-nomenon using simulated phyllotactic patterns with 47 florets, all compared to the same flowerhead.

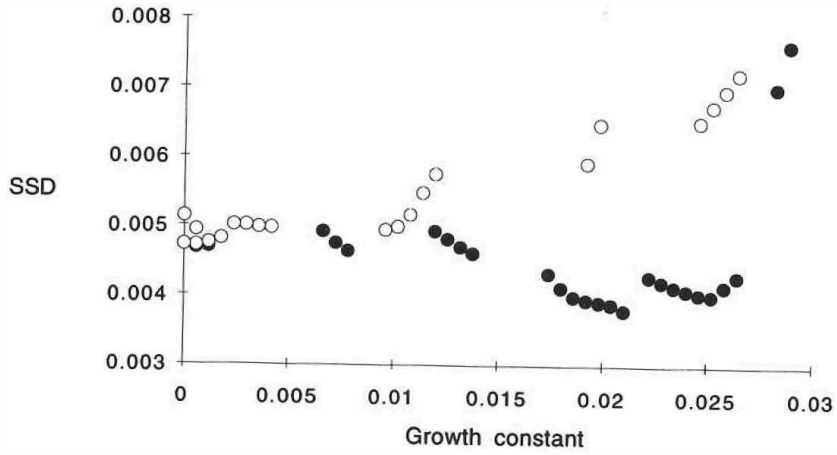

Fig. 15. Deviation (SSD) between an observed flowerhead with 47 primordia and simulated patterns, also with 47 primordia. Light circles represent values obtained for uniformly growing receptacles; dark circles represent values obtained for non-uniformly growing receptacles.

In virtually all size classes, patterns generated using the non-uniform growth model resemble the observed distributions of primordia more closely than patterns generated using the uniform model. This difference is particularly pronounced at

higher growth rates, as indicated in Fig. 15. A possible explanation of this effect is suggested by Figs. 16–18. In the case of uniform growth (Fig. 17), packing of primordia is much less dense at the periphery than in the center of the head. In contrast, the simulated pattern obtained using the non-uniform growth model (Fig. 18) exhibits a more even distribution of florets and in this respect resembles the observed pattern (Fig. 16) more closely.

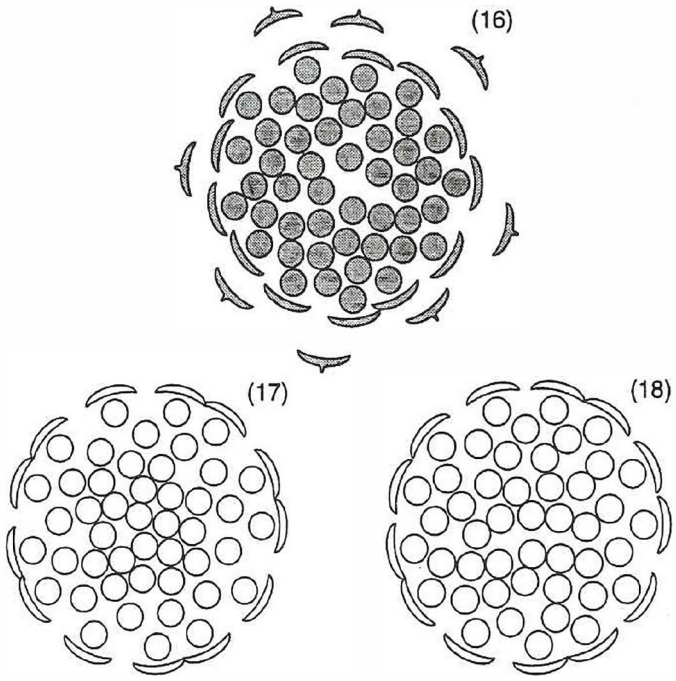

Fig. 16–18. Comparison of floret distribution in heads with equal numbers of florets. (16) A measured *Microseris* head. (17) Simulated head obtained using the uniform growth model (initial radius: 0.91 length units, growth constant: 0.026 length units per plastochron). (18) Simulated head obtained using the non-uniform growth model (initial radius = 1.03 length units, growth constant = 0.026 length units per plastochron).

Figure 19 collects the results of comparisons limited to the outermost 13 primordia for all size classes. These primordia play the dominant role in determining the inner phyllary numbers. The large peaks on the right side of Fig. 19 indicate that combinations of small initial radii with large growth constants lead to unrealistic patterns. Primordia distributions generated using larger initial sizes of the receptacle approximate the observed heads more closely, although there still is much variation in the value of the SSD. Inspection of observed and modeled patterns superimposed on each other gives an insight into some of the reasons for this variation (Figs. 20, 21). Figure 20 presents a good fit between the observed head and the model. In this case, both patterns have 8 inner phyllaries. Further analysis demonstrates that the SSD is also low when both patterns have 13 inner phyllaries.

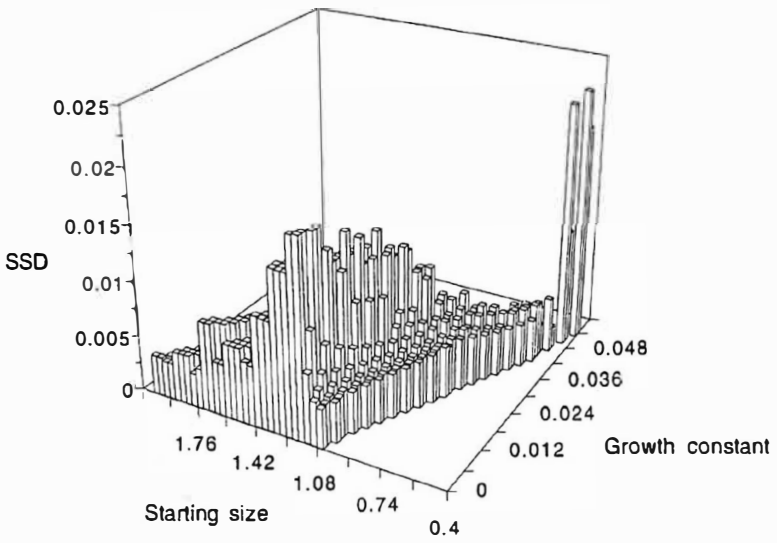

Fig. 19. Deviations (SSD) between the positions of 13 outermost primordia in measured flowerheads and in patterns generated using the modified collision model with non-uniform receptacle growth.

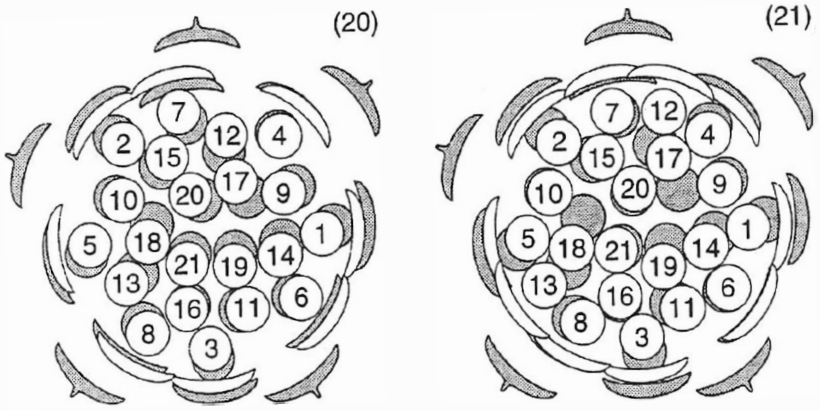

Figs. 20 and 21. Comparisons of the distribution of primordia in a measured *Microseris* head (dark) and in two simulated heads with the same number of primordia. (20) Good fit (SSD = 0.0075) obtained for a simulated head with 8 inner phyllaries (initial radius = 1.0 length units, growth constant = 0.011 length units per plastochron). (21) Poor fit (SSD = 0.0183) obtained for a simulated head with 10 inner phyllaries (initial radius = 0.706 length units, growth constant = 0.0292 length units per plastochron).

In contrast, Fig. 21 illustrates a case of a larger SSD. The modeled head has 10 inner phyllaries, and primordia 12 and 13 are too close to the rim in comparison to the observed head. The effects of this discrepancy propagate towards the center of the modeled head. In conclusion, the predictions of inner phyllary positions

are most realistic for modeled flowerheads with Fibonacci numbers of inner phyllaries.

3.2. *Numbers of Inner Phyllaries and Numerical Canalization*

3.2.1. *Observations*

Eight inbred lines of *Microseris pygmaea* have been used to study naturally occurring genetic variation in meristic characters of flowerheads (Bachmann *et al.*, 1985; Bachmann, 1991). Each inbred line expressed considerable phenotypic plasticity. The number of inner phyllaries per flowerhead was canalized towards Fibonacci numbers while the number of florets varied in a continuous manner. A similar phenotypic plasticity has been found in other species of *Microseris* (Bachmann and Battjes, in press).

The developmental causes of the phenotypic plasticity were studied in two of the inbred lines of *M. pygmaea* by Battjes and Bachmann (1994). In both cases, larger numbers of florets per flowerhead were the result of larger receptacle meristems at the onset of floral initiation. The size of floret primordia was much less variable. The size of the receptacle increased significantly during phyllary and floret formation.

3.2.2. *Simulations*

Figure 22 shows the numbers of inner phyllaries generated by the model for different values of the starting size and the growth constant of the receptacle. Predictably, only Fibonacci numbers of inner phyllaries fit on the rim of a non-growing receptacle. Larger receptacles have higher numbers of phyllaries. With increasing growth constants the preference for Fibonacci numbers of inner phyllaries decreases until, at a growth constant of 0.06 length units per plastochron, no preference for Fibonacci numbers remains. The number of florets increases gradually and shows no preference for Fibonacci numbers (Fig. 23).

3.2.3. *Comparison Results*

The simulation results agree with the records of phenotypic plasticity in *Microseris* flowerheads in the following points:

- the number of inner phyllaries is canalized to Fibonacci numbers whereas the number of florets shows a continuous variation,
- the same (Fibonacci) number of inner phyllaries can occur in receptacles of different initial sizes,
- a considerable growth rate of the receptacle is associated with a frequent occurrence of non-Fibonacci numbers of inner phyllaries.

The model also predicts that receptacles with lower growth rates have more constant numbers of organs on the rim, but we do not yet have the experimental data to verify this prediction.

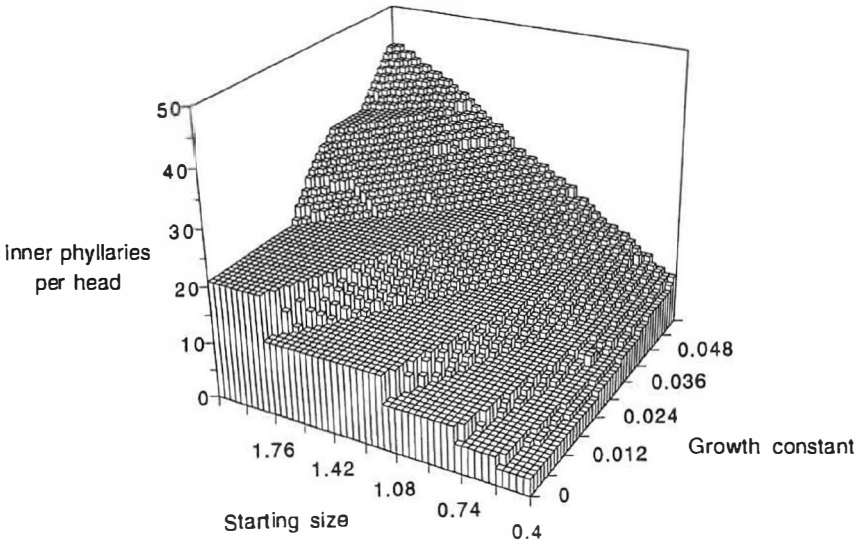

Fig. 22. Number of inner phyllaries per head in 2500 patterns generated using the modified collision model with non-uniform growth of the receptacle.

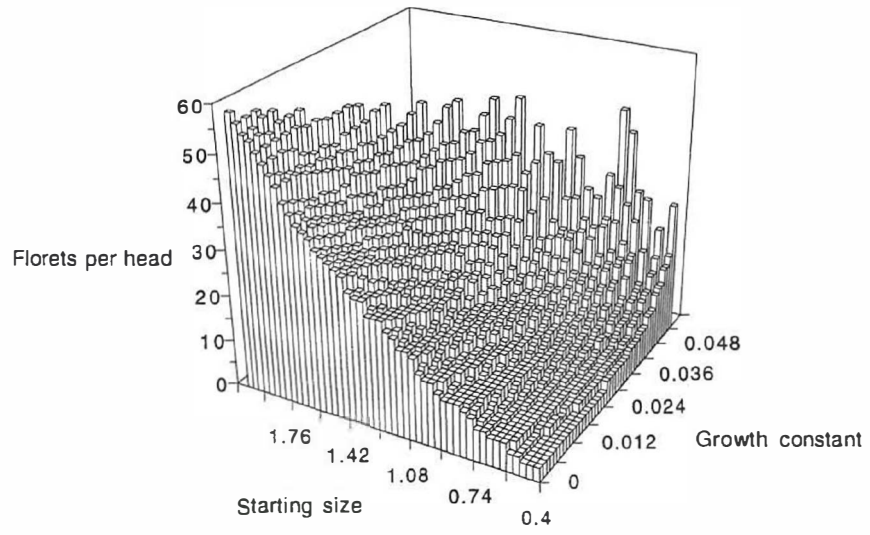

Fig. 23. Numbers of florets per head in 2500 patterns generated using the modified collision model with non-uniform growth of the receptacle. Only values less than 60 are displayed.

3.3. *Ontogenetic Order of Inner Phyllary Positions*

3.3.1. *Observations*

Figure 24 shows the ontogenetic order of inner phyllary positions in the same flowerheads of *M. pygmaea* as described in Sec. 3.3.1. Flowerheads with 8 or 13

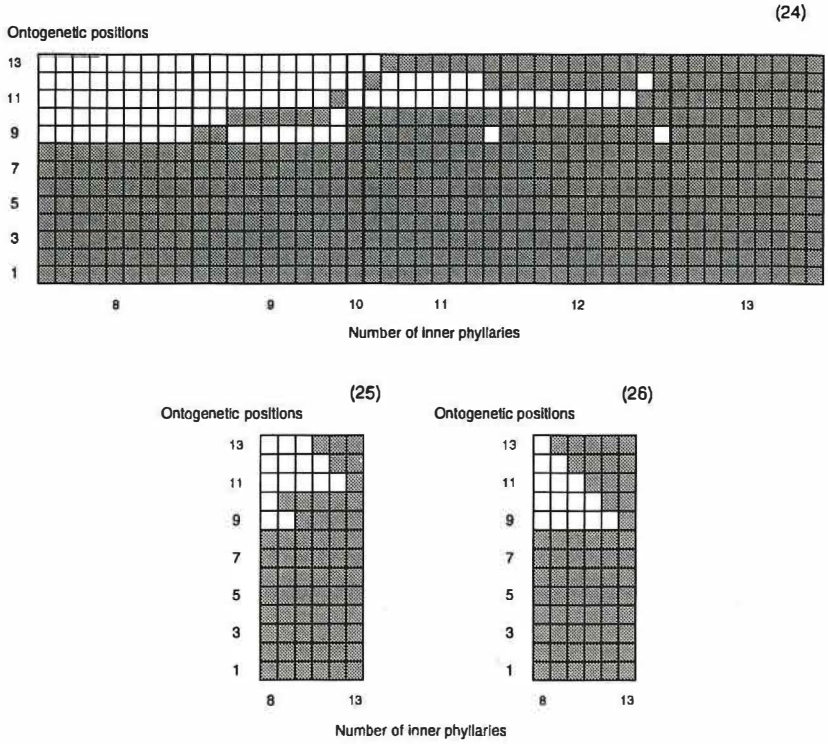

Fig. 24–26. Preferred ontogenetic positions of inner phyllaries. Horizontal axis: number of inner phyllaries per head. Vertical axis: ontogenetic positions occupied by inner phyllaries (dark squares). (24) Results of observations. Each column represents one flowerhead. (25) Summary of observations: the most frequently occupied positions in the observed flowerhead. (26) Inner phyllary positions according to the modified collision model.

inner phyllaries have all first 8 or 13 ontogenetic positions occupied by these phyllaries. An example of a flowerhead with 8 inner phyllaries is shown in Figs. 12 and 13. For numbers of inner phyllaries between 8 and 13, positions 9 and 10 are more often occupied by a phyllary than 11 to 13. Within each of these two groups, however, inner phyllaries at primordium positions *higher* in ontogenetic order occur more frequently. The most frequently observed positions of inner phyllaries are shown in Fig. 25.

3.3.2. *Simulations*

The ontogenetic order of inner phyllaries simulated with the modified collision model follows a peculiar pattern as well (Fig. 26). Patterns with 8 or 13 inner phyllaries have all of the first 8 or 13 ontogenetic positions occupied by the phyllaries. When the number of inner phyllaries is equal to 9, all first 8 positions and position 13 are occupied. With increasing numbers of inner phyllaries, the intermediate positions from 12 to 9 are occupied by inner phyllaries in descending order. Figures 8–11

explain this phenomenon. The first eight primordia fit on the rim and form inner phyllaries. Primordia 9, 10, and 11 do no fit and are displaced toward the center of the receptacle (Figs. 9 and 10). However, since the receptacle increases while the size of primordia remains constant, gaps between primordia become larger as the receptacle expands, and primordia 12 and 13 fit on the rim again (Fig. 11).

3.3.3. *Comparison Results*

The inner phyllaries in the observed flowerheads and the simulated patterns share a tendency to occupy positions of higher ontogenetic order while skipping some positions of lower order, if a non-Fibonacci number of inner phyllaries is present. The agreement of simulations with observations is not complete, because positions 10 and 9 are preferred over 13 to 9 in the observed heads, while positions 13 to 11 are occupied with continuously decreasing preference in modeled heads.

4. Discussion

4.1. *New Insights in Meristic Variation*

The introduction of a growing receptacle and variable divergence angles has made it possible to generate a wider range of phyllotactic patterns than was possible with the original collision model (Fowler *et al.*, 1992). By varying the initial size of the receptacle and the growth rate, we can mimic many patterns of meristic variation observed in *Microseris* and other Asteracean flowerheads (Battjes and Bachmann, in press). Below we discuss these results in detail.

4.1.1. *Spatial Arrangement of Florets on the Receptacle*

We proposed to explain meristic variation in *Microseris* heads as a consequence of the growth of the receptacle during floret initiation. The patterns generated on an expanding receptacle often resembled the observed flowerheads better than patterns generated on a static receptacle.

In order to gain a further insight into the effects of receptacle expansion, we compared two growth modes: uniform growth with a constant relative elementary rate of radius expansion, and non-uniform growth with a growth rate decreasing to zero in the region of the receptacle already occupied by primordia. Phyllotactic patterns generated using the non-uniform model exhibit a higher density of primor-dia distribution at the periphery of the receptacle, and better approximate observed *Microseris* heads. The differential growth appears to be essential in maintaining dense packing of florets across the entire flower head. Nevertheless, the decrease of the elementary growth rate to zero at the periphery is probably unrealistic, and the real values fall between zero and the growth rate characterizing the inner part of the receptacle. Direct measurement of these rates in *Microseris* heads is difficult, because the receptacle is protected by involucral bracts, hairs and leaves during its development.

4.1.2. *Canalization of Inner Phyllary Numbers*

The size of the *Microseris* receptacle may vary while the number of inner phyllaries remains constant. Simulations using the modified collision model agree with this observation. Similarly, variation in growth rate in the model often does not result in a change in the number of organs on the rim. Thus, the modeled algorithm for phyllotactic pattern formation is able to buffer meristic characters against considerable variation in developmental parameters of the receptacle.

The modified collision model also predicts that for smaller ratios of the receptacle growth rate to the primordium initiation rate, the numbers of organs on the rim of the receptacle show less variation. At present we only have a circumstantial confirmation of this prediction. In many whorled flowers the petals appear very quickly one after another in the same sequence as is usually found in flowerheads with spiral phyllotaxis. The meristem growth rate relative to the petal initiation rate is probably low. These flowers often exhibit a Fibonacci number of petals and other floral organs (Endress, 1990). In light of our simulations, we speculate that these two phenomena are connected: the fairly constant number of petals is the consequence of their rapid spiral initiation, combined with slow growth of the meristem. More variable numbers of petals would be a consequence of higher growth rates of the meristem or longer intervals between the initiation of subsequent petals.

4.1.3. *Ontogenetic Order of Inner Phyllaries*

As described in Sec. 3.1.1, inner phyllaries on the *M. pygmaea* flowerheads are distributed in a highly predictable manner. Specifically, position 10 is occupied by a phyllary more frequently than 9, and positions 13 to 11 are occupied in a decreasing order of frequency. The modified collision model exhibits a similar preference for positions higher in ontogenetic order, although the sequence of position occupation is not the same. This preference is a result of packing non-growing primordia on a growing receptacle. Thus, the variation in the positions of inner phyllaries can be largely attributed to geometric relationships between primordia on a growing receptacle.

Although the geometric aspects of incorporating non-growing areas into a growing surface should be further analyzed, there are good reasons for keeping the size of primordia constant during the simulations. Floret primordia of *M. pygmaea* measured during several consecutive days of flowerhead development do not show a significant increase in size, although the receptacle expands considerably (Battjes and Bachmann, 1994). This indicates that rates of expansion may indeed be different between florets and the receptacle. Furthermore, the developmental mechanism that creates phyllotactic patterns on the receptacle may be of a chemical rather than mechanical nature. If this is the case, the primordium size used in the model could be re-interpreted as the radius of an inhibitory field created by the primordium; the size of this field may be independent of the actual primordium size and receptacle growth.

4.2. *Suggestions for Future Work*

The present study suggests several topics for future research that may contribute to a better understanding of the geometric aspects of meristic variation and spiral phyllotaxis.

- The proposed model postulates that the distribution of florets on the receptacle and the canalization of inner phyllaries are influenced by the growth of the receptacle, with differential growth rates leading to a better agreement between the model and the observations of the *Microseris* flowerheads. A direct confirmation of this relationship by measurements of the relative elementary growth rate in different zones of the receptacle over time would significantly contribute to model validation.

- It is an interesting question, how the developmental fate of primordia can be controlled by apparently very small deviations in their positions. A more detailed analysis of these positions, for example expressed in relation to the closest neighboring primordia rather than in absolute coordinates, may provide a useful insight.

- The modified collision model does not predict the observed difference in chance to become an inner phyllary between primordia 10–9 and 13–12. Also, for a non-Fibonacci number of the inner phyllaries, some inner phyllary primordia in the model are too close to the rim (see Sec. 3.1.4). These shortcomings require an explanation. For example, our view of collisions between neighboring primordia may be too simplistic, and more complicated interactions involving several neighboring primordia may have to be considered. Such a different approach might lead to other divergence angles and collision patterns, and consequently to other arrangements of the inner phyllaries.

- An important question is the applicability of the results of the present study to a wide range of Asteracean species. Although there is no indication that the described distribution of inner phyllaries and florets is specific to *Microseris*, it is important to confirm that other species can be characterized by the same model, possibly with different values of parameters.

- The divergence angle of 137.5° between sequentially placed primordia is assumed both in the original collision model and its modification presented in this paper, although in the latter case the angle is adjusted as a result of interactions between neighboring primordia. Ideally, this value should not be given *a priori*, but should result from the model. Models in which the divergence angle is an emergent property have been described in literature (Mitchison, 1977; Douady and Couder, 1992; Van der Linden, 1994; Yotsumoto, 1993; Koch and Meinhardt, 1994), but they are in turn limited in their capability of explaining meristic variation. It would be of great importance to develop a model of phyllotaxis, in which:

the sequence of primordia placement and the divergence angle are not assumed, but result from simulations, and

the power of the modified collision model to explain the meristic variation and the departure from the ontogenetic order in inner phyllary formation is preserved.

4.3. *Concluding Remarks*

Spiral phyllotactic patterns have often been idealized as extremely regular, with the divergence angle constant or changing gradually, and the distance from the primordia to the center decreasing in a continuous manner (e.g. Erickson, 1983). In the same manner, larger flowerheads have been viewed as differing from smaller ones only by the addition of extra florets at the periphery (Vogel, 1979; Bursill and Fan Xudong, 1988; van der Linden, 1990). Although these approximations may be adequate for many purposes, they promote a simplified view of phyllotaxis. Divergence angles in flowerheads are not constant but show regular, non-random deviations from the average (Ryan *et al.*, 1991, Battjes *et al.*, 1993). The distances from primordia to the head center change discontinuously (Battjes *et al.*, 1993). In the present study we have further shown that primordia on the rim of a *Microseris* head have different chances of developing into an inner phyllary, which are out of step with the ontogenetic order. These deviations from abstract spiral or helical patterns are typical properties of flowerhead phyllotaxis rather than exceptions. We believe that they can be best understood by taking ontogenesis of the phyllotactic pattern into account, integrating postulated developmental mechanisms into a computer model, and carefully comparing the results with observations.

Acknowledgements

We would like to thank Lynn Mercer for help with the proof of Hirmer's conjecture, and Chris Prusinkiewicz for proofreading the manuscript. The anatomical observations were performed in the Hugo de Vries Laboratory of the University of Amsterdam. We thank Ferry Bouman and Konrad Bachmann for providing the facilities. All simulations were carried out in the Computer Graphics Laboratory at the University of Calgary. Johannes Battjes was supported in part by a NATO Science Fellowship awarded by the Netherlands Organization for Scientific Research (NWO). Przemyslaw Prusinkiewicz was supported in part by research and equipment grants from the Natural Sciences and Engineering Research Council of Canada (NSERC) and from Apple Computer. All support is gratefully acknowledged.

Appendix A: Proof of Hirmer's Conjecture

Hirmer (1931) proposed an explanation for the canalization of the numbers of organs n found at the perimeter of flowerheads. His explanation was based on the postulate that n is the maximum number of primordia of a given size that fit on

the circular rim of a receptacle without intersecting each other. Hirmer observed that if the divergence angle between consecutively placed primordia is equal to the golden angle φ (approximately 137.5°), n is a Fibonacci number for any ratio of the primordium radius r to the rim radius R. Although this observation was later supported by calculations of special cases and computer simulations (Battjes 1994), to our knowledge it has not been formally proved. The purpose of this appendix is to present such a proof.

Let us consider a set $\mathcal{P}^{(n)}$ of n distinct points representing the centers of primordia placed on the rim of a receptacle. We will arrange this set into two sequences. The *ontogenetic sequence*, denoted $\{P_i\}$ describes the order in which the sequentially generated points $P_1, P_2, \ldots, P_n$ have been placed on the rim. It is assumed that pairs of consecutive points P_i form a constant *divergence angle* ψ when seen from the rim center O:

$$\angle P_i O P_{i+1} = \psi \quad \text{for} \quad i = 1, 2, \ldots, n-1 . \tag{4}$$

The *partitioning sequence*, denoted $\{P_{p_j}\}$, is a permutation of the sequence $\{P_i\}$ such that $P_{p_1} = P_1$ and $P_{p_1}, P_{p_2}, \ldots, P_{p_n}$ are consecutive points encountered while traversing the rim counterclockwise:

$$0 < \angle P_{p_1} O P_{p_2} < \angle P_{p_1} O P_{p_3} < \cdots < \angle P_{p_1} O P_{p_n} < 360° . \tag{5}$$

We will denote by $\Xi^{(n)}_{p \to o} : \{1, 2, \ldots, n\} \to \{1, 2, \ldots, n\}$ the function that converts the index p_j of a point P in the partitioning sequence $\{P_{p_j}\}$ to the index i of the same point in the ontogenetic sequence $\{P_i\}$.

The partitioning sequence divides the full angle into n *partition angles*:

$$\angle P_{p_1} O P_{p_2} \ , \ \angle P_{p_2} O P_{p_3} \ , \ldots , \ \angle P_{p_{n-1}} O P_{p_n} \ , \ \angle P_{p_n} O P_{p_1} . \tag{6}$$

We will denote the set of (different) values of these angles by $A^{(n)}$. The notions introduced above are illustrated in Fig. 27.

Lemma 1. Let $\mathcal{S}$ be an infinite ontogenetic sequence of points $P_1, P_2, P_3, \ldots$ generated using a divergence angle ψ:

$$\angle P_i O P_{i+1} = \psi \quad \text{for} \quad i = 1, 2, 3, \ldots . \tag{7}$$

If ψ is an irrational number, there exists an infinite set of integers $\mathcal{N}$ such that for any $n \in \mathcal{N}$, the set of points $\mathcal{P}^{(n)}$ satisfies the conditions:

1. $\mathcal{P}^{(n)}$ consists of n initial elements of the sequence $\mathcal{P}$,
2. the set $A^{(n)}$ of the values of partition angles has two elements,
3. the two partition angles sharing the vertex $P_{p_1} = P_1$ are different: $\angle P_{p_n} O P_{p_1} \neq \angle P_{p_1} O P_{p_2}$.

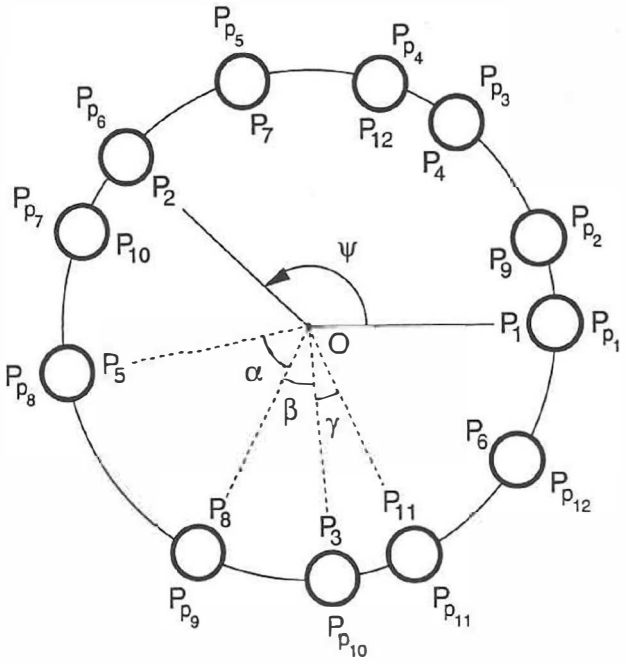

Fig. 27. The ontogenetic sequence (labeled inside the rim) and the partitioning sequence (labeled outside) of $n = 12$ points, generated using the divergence angle $\psi = 137.5°$. The function $\Xi^{(12)}_{p\to o}$ converts the indices of points in the partitioning sequence to the indices of points in the ontogenetic sequence; for example, $\Xi^{(12)}_{p\to o}(1) = 1$, $\Xi^{(12)}_{p\to o}(2) = 9$, $\Xi^{(12)}_{p\to o}(6) = 2$. The set $A^{(12)}$ of partition angle values has three elements α, β and γ.

Proof: by induction on n.

Initial step. For $n = 2$ the set $\mathcal{P}^{(n)}$ consists of two points P_1 and P_2. There are two partition angles, $\angle P_1OP_2$ and $\angle P_2OP_1$, which have different values (otherwise the divergence angle ψ would have been equal to 180°, which is a rational number) and share point P_1.

Inductive step. Assume that the thesis is true for some $n \geq 2$. Let $\angle P_{p_n}OP_{p_1} = \alpha$ and $\angle P_{p_1}OP_{p_2} = \beta$, with $\alpha > \beta$ (the opposite case can be considered in a similar way). Rotate $P_1, P_2, \ldots, P_n$ with respect to the receptacle center O by angle β and label the resulting points $Q_1, Q_2, \ldots, Q_n$, respectively. Denote the set $\{Q_1, Q_2, \ldots, Q_n\}$ by $\mathcal{Q}^{(n)}$. Refer to Fig. 28 for an illustration of the proof.

1. Observe that the rotation of point P_1 by β makes the resulting point Q_1 coincide with the point P_{p_2}. Denote by $k+1$ $(k \geq 1)$ the index of the point P_{p_2} in the ontogenetic sequence:

$$k + 1 = \Xi^{(n)}_{p\to o}(p_2)\,. \tag{8}$$

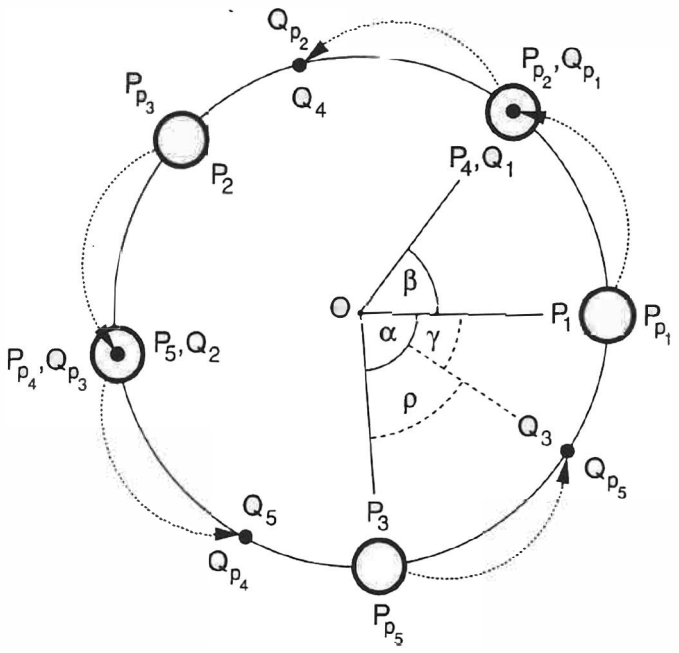

Fig. 28. Illustration of the proof of Lemma 1. Small circles represent points of the set $\mathcal{P}^{(5)}$, generated using the divergence angle of 137.5°. Dots represent points of the set $\mathcal{Q}^{(5)}$, obtained by rotating points $P_i \in \mathcal{P}^{(5)}$ by angle β with respect to the receptacle center O, as indicated by the dashed arrows.

Since the divergence angle between consecutive points in the sequences $\{Q_i\}$ is the same as in the sequence $\{P_i\}$, we obtain:

$$Q_1 = P_{k+1}\,,\; Q_2 = P_{k+2}\,,\ldots,\; Q_{n-k} = P_n\,,\ldots,\; Q_n = P_{n+k}\,. \tag{9}$$

The first $n-k$ points of the sequence $\{Q_i\}$ coincide with the last $n-k$ points of the sequence $\{P_i\}$ included in the set $\mathcal{P}^{(n)}$. The remaining $k \geq 1$ points of the sequence $\{Q_i\}$ are equal to the elements $P_{n+1}, P_{n+2}, \ldots, P_{n+k}$ of the sequence $\mathcal{S}$ not included in $\mathcal{P}^{(n)}$. Consequently, the set $\mathcal{P}^{(n)} \cup \mathcal{Q}^{(n)} = \mathcal{P}^{(n+k)}$ consists of $n+k > n$ initial points of the sequence $\mathcal{S}$.

2. Consider the merged sequence

$$P_{p_1}, Q_{p_1}, P_{p_2}, Q_{p_2}, \ldots, P_{p_n}, Q_{p_n} \tag{10}$$

and assume formally that $P_{p_1} = P_{p_{n+1}}$ and $Q_{p_1} = Q_{p_{n+1}}$. From the construction of points $Q_{p_1}, Q_{p_2}, \ldots, Q_{p_n}$ it follows that $\angle P_{p_i} O Q_{p_i} = \beta$ for any $i = 1,2,\ldots,n$. On the other hand, from the inductive assumption it follows that $\angle P_{p_i} O P_{p_{i+1}} \in \{\alpha, \beta\}$ for any $i = 1,2,\ldots,n$. Two cases may occur:

- if $\angle P_{p_i} O P_{p_{i+1}} = \alpha$ then point Q_{p_i} lies between points P_{p_i} and $P_{p_{i+1}}$, and the angle $\angle P_{p_i} O P_{p_{i+1}}$ is divided into two smaller angles:

$$\angle P_{p_i} O Q_{p_i} = \beta \quad \text{and} \quad \angle Q_{p_i} O P_{p_{i+1}} = \alpha - \beta = \gamma . \tag{11}$$

- if $\angle P_{p_i} O P_{p_{i+1}} = \beta$ then points Q_{p_i} and $P_{p_{i+1}}$ coincide;

Consequently, the merged sequence (10) consists of points of the set $\mathcal{P}^{(n+k)} = \mathcal{P}^{(n)} \cup \mathcal{Q}^{(n)}$ listed in the partitioning order, although some points may be listed twice. From the equalities (11) it follows that the set $A^{(n+k)}$ of partition angles for the set of points $\mathcal{P}^{(n+k)}$ has two elements: β and γ.

3. According to the partitioning sequence (10), the vertex P_{p_1} is shared by the angles $\angle Q_{p_n} O P_{p_1}$ and $\angle P_{p_1} O Q_{p_1}$. From the assumptions $\angle P_{p_n} O P_{p_1} = \alpha$ and $\angle P_{p_1} O P_{p_2} = \beta$ it follows that

$$\begin{aligned} &\angle Q_{p_n} O P_{p_1} = \angle P_{p_n} O P_{p_1} - \angle P_{p_n} O Q_{p_n} = \alpha - \beta = \gamma , \\ &\angle P_{p_1} O Q_{p_1} = \beta . \end{aligned} \tag{12}$$

The angles β and γ are not equal; otherwise the divergence angle ψ and the full angle 360° could be both expressed as integer multiples of γ and ψ would be a rational number. Thus, the set $\mathcal{P}^{(n+k)}$ satisfies conditions 1 — 3 of the thesis for $n + k > n$. □

We will now focus on the special case in which the divergence angle ψ is equal to the golden angle $\varphi = 360°(1-\tau)$. The golden ratio τ is defined by the equations:

$$\frac{\tau}{1} = \frac{1-\tau}{\tau} \quad \text{or} \quad \tau^2 = 1 - \tau . \tag{13}$$

Lemma 2. If $\theta_1 = 360°\tau$, $\theta_2 = 360°(1-\tau)$, and $\theta_{i+1} = \theta_{i-1} - \theta_i$ for $i \geq 2$, then $\theta_i = 360°\tau^i$ for any $i \geq 1$.

Proof: by induction on i.

Initial step. Obviously, $\theta_1 = 360°\tau = 360°\tau^1$ and $\theta_2 = 360°(1-\tau) = 360°\tau^2$.

Inductive step. Assume that the thesis is true for some $i \geq 2$. For $i+1$ we obtain:

$$\begin{aligned} \theta_{i+1} &= \theta_{i-1} - \theta_i = 360°(\tau^{i-1} - \tau^i) = 360°\tau^{i-1}(1-\tau) \\ &= 360°\tau^{i-1}\tau^2 = 360°\tau^{i+1} . \quad \square \end{aligned} \tag{14}$$

Lemma 3. If the divergence angle ψ is equal to the golden angle φ, then:

1. the set $\mathcal{N}$ of integers $n_1 < n_2 < n_3 < \cdots$ satisfying Lemma 1 consists of consecutive elements of the Fibonacci sequence: $f_1 = f_2 = 1$, $f_{i+2} = f_{i+1} + f_i$ for $i \geq 1$, starting with $n_1 = f_3 = 2$;

2. for any $i \geq 1$ the partitioning sequence of points in $\mathcal{P}^{(n_i)}$ divides the full angle into f_{i+1} angles $\theta_i = 360°\tau^i$ and f_i angles $\theta_{i+1} = 360°\tau^{i+1}$.

3. for any $0 < m < n_{i+1} - n_i$, the partitioning sequence of points in $\mathcal{P}^{n_i+m}$ divides the full angle into $f_{i+1} - m$ angles $\theta_i = 360°\tau^i$, $f_i + m$ angles $\theta_{i+1} = 360°\tau^{i+1}$, and m angles $\theta_{i+2} = 360°\tau^{i+2}$, with all three angle values occurring at least once.

Proof: by induction on i.

Initial step. By definition, the set $\mathcal{P}^{(n_1)}$ consists of $f_3 = 2$ points P_1 and P_2 such that

$$\angle P_1OP_2 = \varphi = \theta_2 \quad \text{and} \quad \angle P_2OP_1 = 360 - \varphi = \theta_1 \tag{15}$$

There is no integer m satisfying the inequality $0 < m < n_2 - n_1 = 3 - 2 = 1$, thus part 3 of the thesis also holds.

Inductive step. Assume that the thesis is true for some $i \geq 1$. Construct the set $\mathcal{P}^{(n_i+k)}$ as described in the proof of Lemma 1. From Lemma 2 it follows that $\theta_i > \theta_{i+1}$, thus the partitioning sequence of points in $\mathcal{P}^{(n_i+k)}$ divides the full angle into $f_i + f_{i+1} = f_{i+2}$ angles θ_{i+1} and f_{i+1} angles $\theta_i - \theta_{i+1} = \theta_{i+2}$. For any $0 < m < f_{i+1}$, the partitioning sequence of points in $\mathcal{P}^{(n_i+m)}$ subdivides only m of the f_{i+1} angles θ_i into θ_{i+1} and θ_{i+2}, thus the full angle is subdivided into $f_{i+1} - m$ angles θ_i, $f_i + m$ angles θ_{i+1}, and m angles θ_{i+2}. Consequently, the sequence $\mathcal{N}$ has no elements between $n_i = f_{i+2}$ and $n_{i+1} = f_{i+2} + f_{i+1} = f_{i+3}$. □

Theorem (Hirmer's conjecture). Let D be a circle with center O and radius R. Consider the largest set of circles $\mathcal{C}^{(n)} = C_1, C_2, \ldots, C_n$, with the set of centers $\mathcal{P}^{(n)} = \{P_1, P_2, \ldots, P_n\}$, such that:

1. all points $P_i \in \mathcal{P}^{(n)}$ lie on the circumference of the circle D,

2. for any $i = 1, 2, \ldots, n-1$, the divergence angle $\angle P_iOP_{i+1}$ is the golden angle φ,

3. all circles $C_i \in \mathcal{C}^{(n)}$ have the same radius $r < R$,

4. no two different circles $C_i, C_j \in \mathcal{C}$ intersect.

The number n of circles in the set $\mathcal{C}^{(n)}$ is a Fibonacci number.

Proof. Circles $C_i, C_j \in \mathcal{C}^{(n)}$ will not intersect if the distance between their centers satisfies the inequality $|P_iP_j| > 2r$, or $\angle P_iOP_j > \zeta = 2\arcsin\frac{r}{R}$ (Fig. 29). Let θ_{i+1} be the smallest element of the sequence $\{\theta_i\}$ (see Lemma 2), such that $\theta_{i+1} > \zeta$. According to Lemma 3, a Fibonacci number n_i is the largest number of points satisfying assumptions 1 and 2 above, such that the partitioning sequence of points in $\mathcal{P}^{(n_i)}$ does not include an angle less than or equal to ζ. □

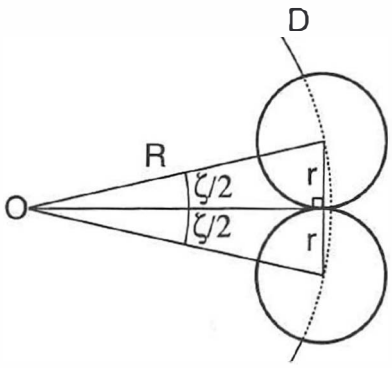

Fig. 29. Definition of angle ζ.

Appendix B: Minimizing the Sum of the Squared Distances between Corresponding Primordium Positions

In the scope of this paper, we are interested in the layout of primordia on receptacles, and we abstract from differences in position, orientation, and size of the resulting patterns. Consequently, when comparing two patterns, we select one as a template, and transform the other until the best match possible has been achieved. In this appendix, we derive parameters of transformations that result in the optimal match.

The quality of the match is measured as the sum of squared distances (ssd) between the corresponding primordia in the template pattern a and the transformed pattern b':

$$\text{ssd} = \sum_{i=1}^{n} \left[(x_{ai} - x_{b'i})^2 + (y_{ai} - y_{b'i})^2 \right] \tag{16}$$

The coordinates x_{ai} and y_{ai} indicate positions of floret primordia in pattern a, and $x_{b'i}$ and $y_{b'i}$ indicate positions of primordia in pattern b after the transformation. The upper summation limit n determines the number of primordia being compared and must not exceed the total number of primordia in either pattern. A smaller value of n is used when we are interested in comparing only a limited number of primordia in the flowerheads. The index $i = 1, 2, \ldots, n$ identifies primordia numbers in the ontogenetic sequence. It is assumed that in both patterns all primordia from 1 to n are present (in other words, all coordinates x_{ai}, y_{ai} and x_{bi}, y_{bi} are defined).

The cumulative effect of any combination of translations, rotations, and scalings can be expressed as the composition of a translation by vector $\vec{k}$ along the x axis of the underlying coordinate system, a translation by vector $\vec{l}$ along the y axis, a rotation by angle α around the origin of the coordinate system, and scaling by factor s with respect to the same point. This composite transformation is then captured by the formulae (see Foley *et al.*, 1990, Chapter 5):

$$\begin{aligned} x_{b'i} &= (x_{bi} + k)s\cos\alpha - (y_{bi} + l)s\sin\alpha\,, \\ y_{b'i} &= (x_{bi} + k)s\sin\alpha + (y_{bi} + l)s\cos\alpha\,. \end{aligned} \tag{17}$$

After substituting the right hand sides of Eq. 17 for $x_{b'i}$ and $y_{b'i}$ in Eq. 16, the ssd becomes a function of parameters k, l, α, and s. Since the purpose of transforming pattern b is to determine the best match possible between a and the resulting pattern b', we seek parameter values for which the ssd reaches minimum. According to elementary calculus, the necessary condition is that the partial derivatives of the ssd with respect to all parameters are equal to zero. To simplify the calculations, we assume that the center of gravity of pattern a lies at the origin of the coordinate system:

$$\sum_{i=1}^{n} x_{ai} = \sum_{i=1}^{n} y_{ai} = 0\,. \tag{18}$$

Since it is always possible to position pattern a in such a manner that this assumption is satisfied, no generality is lost.

Considering the translations first, we obtain:

$$\frac{\partial \mathrm{ssd}}{\partial k} = 2s^2 \sum_{i=1}^{n} (x_{bi} + k)\,, \tag{19}$$

thus, disregarding the degenerated case $s = 0$,

$$\frac{\partial \mathrm{ssd}}{\partial k} = 0 \quad \text{if} \quad k = \frac{1}{n}\sum_{i=1}^{n} x_{bi}\,. \tag{20}$$

Similarly,

$$\frac{\partial \mathrm{ssd}}{\partial l} = 0 \quad \text{if} \quad l = \frac{1}{n}\sum_{i=1}^{n} y_{bi}\,. \tag{21}$$

The derivative with respect to the angle α is equal to:

$$\frac{\partial \mathrm{ssd}}{\partial \alpha} = 2s\sin\alpha \sum_{i=1}^{n} (x_{ai}x_{bi} + y_{ai}y_{bi}) - 2s\cos\alpha \sum_{i=1}^{n} (x_{bi}y_{ai} - x_{ai}y_{bi})\,, \tag{22}$$

thus, assuming that $s \neq 0$ and that no division by zero is performed, we obtain:

$$\frac{\partial \mathrm{ssd}}{\partial \alpha} = 0 \quad \text{if} \quad \alpha = \arctan \frac{\left[\sum_{i=1}^{n} (x_{bi}y_{ai} - x_{ai}y_{bi})\right]}{\left[\sum_{i=1}^{n} (x_{ai}x_{bi} + y_{ai}y_{bi})\right]}\,. \tag{23}$$

If the denominator in the above formula is equal to 0, we use the value $\alpha = \frac{\pi}{2}$, determined directly from Eq. 22.

In order to calculate the derivative of Eq. 16 with respect to the scale s, we introduce auxiliary variables:

$$\begin{aligned} \tilde{x}_{bi} &= (x_{bi} + k)\cos\alpha - (\tilde{y}_{bi} + l)\sin\alpha\,, \\ \tilde{y}_{bi} &= (x_{bi} + k)\sin\alpha + (\tilde{y}_{bi} + l)\cos\alpha\,. \end{aligned} \tag{24}$$

From Eq. 17 it follows that $x'_{bi} = s\tilde{x}_{bi}$ and $y'_{bi} = s\tilde{y}_{bi}$. By substituting the right-hand sides of these formulae into Eq. 16, we obtain:

$$\frac{\partial \text{ssd}}{\partial s} = 2s\sum_{i=1}^{n}(\tilde{x}_{bi}^2 + \tilde{y}_{bi}^2) - 2\sum_{i=1}^{n}(x_{ai}\tilde{x}_{bi} + y_{ai}\tilde{y}_{bi})\,. \tag{25}$$

As a result,

$$\frac{\partial \text{ssd}}{\partial s} = 0 \quad \text{if} \quad s = \frac{\sum_{i=1}^{n}(x_{ai}\tilde{x}_{bi} + y_{ai}\tilde{y}_{bi})}{\sum_{i=1}^{n}(\tilde{x}_{bi}^2 + \tilde{y}_{bi}^2)}\,. \tag{26}$$

Further inspection reveals that the ssd reaches the minimum for the values of parameters k, l, and s determined by Eqs. 20, 21, and 26 respectively. The value of α obtained using Eq. 23 corresponds to either a minimum or a maximum of the ssd. In the case of a maximum, π should be added to α to obtain the minimum.

In the paper, we often refer to a normalized version of the ssd, defined by the equation:

$$\text{SSD} = \frac{\text{ssd}}{\text{radius}(a)\ \text{radius}(b)\ n}\,. \tag{27}$$

The purpose of dividing the ssd by the radii of patterns a and b and the number n is to make the resulting value more suitable for comparisons involving receptacles of different sizes and with different numbers of primordia.

References

Bachmann K., Evolutionary genetics and the genetic control of morphogenesis in flowering plants, *Evol. Biol.* **15** (1983) 157–208.

Bachmann K., Genetic variation for meristic characters of the capitula of *Microseris pygmaea* (Asteraceae: Lactuceae), *Biol. Zentr. Bl.* **110** (1991) 145–156. Bachmann K. and Chambers K. L., Heritable variation for heterocarpy in *Microseris bigelovii* (Asteraceae-Lactuceae), *Beitr. Biol. Pfl.* **65** (1990) 123–146.

Bachmann K., Chambers K. L., Grau J. and Price H. J., Genetic variation in *Microseris pygmaea* (Asteraceae-Lactuceae), *Beitr. Biol. Pfl.* **60** (1985) 51–88.

Battjes J., *Determination of Organ Numbers During Inflorescence Development of Microseris* (Asteraceae: Lactuceae), Ph.D. Thesis, University of Amsterdam.

Battjes J. and Bachmann K., Phenotypic plasticity of capitulum morphogenesis in *Microseris pygmaea* (Asteraceae: Lactuceae), *Ann. Bot.* **73** (1994) 299–305.

Battjes J. and Bachmann K., Numerical canalization in asteracean heads. In: *Compositae: Biology and Utilization*, ed. by N. Hind, in press.

Battjes J., Bachmann K. and Bouman F., Early development of capitula in *Microseris pygmaea* D. don strains C96 and A92 (Asteraceae: Lactuceae), *Bot. Jahrb. Syst.* **113** (1992) 461–475.

Battjes J., Vischer N. O. E. and Bachmann K., Capitulum phyllotaxis and numerical canalization in *Microseris pygmaea* (Asteraceae: Lactuceae), *Amer. J. Bot.* **80** (1993) 419–428.

Brown P. H. and Menary R. C., Changes in apical morphology during floral initiation and development in pyrethrum (*Tanacetum cinerariaefolium* L), *J. Hort. Sci.* **69** (1994) 181–188.

Bursill L. A. and Fan Xudong, Close packing of growing discs, *Mod. Phys. Lett.* **B2** (1988) 1245–1252.

Church A. H., *On the Relation of Phyllotaxis to Mechanical Laws*, **Part I and II** (Williams and Norgate, London, 1902).

Coen E. S. and Carpenter R., The Metamorphosis of flowers, *Plant Cell* **5** (1993) 1175–1181.

Dormer K. J., *Shoot Organization in Higher Plants* (Chapman and Hall, London, 1972).

Douady S. and Couder Y., Phyllotaxis as a physical self-organized growth process, *Phys. Rev. Lett.* **68** (1992) 2098–2101.

Endress P. K., Floral phyllotaxis and floral evolution, *Bot. Jahrb. Syst.* **108** (1987) 417–438.

Endress P. K., Patterns of floral construction in ontogeny and phylogeny, *Biol. J. Linn. Soc.* **39** (1990) 153–175.

Endress P. K., Evolution and floral diversity: the phylogenetic surroundings of *Arabidopsis* and *Antirrhinum*, *Int. J. Plant Sci.* **153S** (1992) 106–122.

Erickson R. O. and Sax K. B., Elementary growth rate of the primary root of *Zea mays*, *Proc. Amer. Phil. Soc.* **100** (1956) 487–498.

Erickson R. O., The geometry of phyllotaxis. In: *The Growth and Functioning of Leaves*, ed. by Dale J. E. and Milthorpe F. L. (Cambridge Univ. Press, Cambridge, 1983).

Foley, J. D., van Dam A., Feiner S. K., and Hughes J. F., *Computer Graphics. Principles and Practice*, 2nd ed. (Addison-Wesley, Reading, 1990).

Fowler D., Prusinkiewicz P. and Battjes J., A collision-based model of spiral phyllotaxis, *Computer Graphics* **26** (1992) 361–368.

Green P. B. and King A., A mechanism for the origin of specifically oriented textures in development with special reference to *Nitella* wall texture. *Aust. J. Biol. Sci.* **19** (1966) 421–437.

Hirmer M., Zur Kenntnis der Schraubenstellungen im Pflanzenreich, *Planta* **14** (1931) 132–206.

Horridge J. S. and Cockshull K. E., Size of the *Chrysanthemum* shoot apex in relation to inflorescence initiation and development, *Ann. Bot.* **44** (1979) 547–556.

Huether C. A., Exposure of natural genetic variability underlying the pentamerous corolla constancy in *Linanthus androsaceus* ssp. *androsaceus*, *Genetics* **60** (1968) 123–146.

Jean R. V., *Phyllotaxis, a Systemic Study in Plant Morphogenesis* (Cambridge Univ. Press, Cambridge, 1994).

King R. M. and Robinson H., The genera of the eupatorieae (Asteraceae), *Mon. Syst. Bot. Miss. Bot. Gard.* **22** (1987) 1–581.

Koch A. J. and Meinhardt H., Biological pattern formation: from basic mechanisms to complex structures, 1994.

Leppik E. E., The evolution of capitulum types of the compositae in the light of insect-flower interaction. In: *The Biology and Chemistry of the Compositae*, ed. by Heywood V. H., Harborne J. B. and Turner B. L., (Academic Press, London, 1977) pp. 61–90.

Ludwig F., Die Anzahl der Strahlenblüten bei *Chrysanthemum leucanthemum* und anderen Kompositen, *D. Bot. Monatssch.* **5** (1887) 52–58.

Meicenheimer R. D., Relationships between shoot growth and changing phyllotaxy of *Ranunculus*, *Amer. J. Bot.* **66** (1979) 557–569.

Mitchison G. J., Phyllotaxis and the Fibonacci series, *Science* **196** (1977) 270–275.

Palmer J. H. and Steer B. T., The generative area as the site of floret initiation in the sunflower capitulum and its integration to predict floret number, *Field Crops Res.* **11** (1985) 1–12.

Popham R. H. and Chan A. P., Origin and development of the receptacle of *Chrysanthemum morifolium*, *Amer. J. Bot.* **39** (1952) 329–339.

Rauh W. and Reznik H., Histogenetische Untersuchungen an Büten- und Infloreszenzachsen II. Die Histogenese der Achsen köpchenförmiger Infloreszenzen, *Beitr. Biol. Pfl.* **29** (1953) 233–296.

Ryan G. W., Rouse J. L. and Bursill L. A., Quantitative analysis of sunflower seed packing, *J. Theor. Biol.* **147** (1991) 303–328.

Sharman K. V. and Sedgley M., Floral initiation and development in *Helipterum roseum* (Hook.) Benth. and *Helichrysum bracteatum* (Vent.) Andrews (Asteraceae), *Aust. J. Bot.* **36** (1988) 575–587.

Szymanowska-Pulka J., Phyllotactic patterns in capitula of *Carlina acaulis L.*, *Acta Soc. Bot. Pol.* **63** (1994) 229–245.

van der Linden F. M. J., Creating phyllotaxis, the dislodgement model, *Math. Biosci.* **100** (1990) 161–199.

van der Linden F. M. J., *Phyllotactic Patterns for Domes*, Ph.D. Thesis, University of Eindhoven, The Netherlands, (1994).

Vlot E. C., van Houten W. H. J., Mauthe S. and Bachmann K., Genetic and non-genetic factors influencing deviations from five pappus parts in a hybrid between *Microseris douglasii* and *M. bigelovii* (Asteraceae, Lactuceae), *Int. J. Plant Sci.* **153** (1992) 89–97.

Vogel H. A., A better way to construct the sunflower head, *Math. Biosci.* **44** (1979) 179–189.

Weyl H., *Symmetry.* (Princeton Univ. Press, Princeton, 1952, 1982).

Weisse A., Die Zahl der Randblüthen an Compositenköpfchen in ihrer Beziehung zur Blattstellung und Ernährung, *Jahrb. Wiss. Bot.* **30** (1897) 453–483.

Yotsumoto A. A., A diffusion model for phyllotaxis, *J. Theor. Biol.* **162** (1993) 131–151.